crystals

MDPI

Article

Magnesium-Containing Silicate Bioceramic Degradable Intramedullary Nail for Bone Fractures

Yuxiang Ye [1,†], Huifeng Shao [1,2,3,4,*,†], Zhuoluo Jing [1,†], Zhiheng Nian [1] and Youping Gong [1]

[1] School of Mechanical Engineering, Hangzhou Dianzi University, Hangzhou 310018, China; yyx15157973928@163.com (Y.Y.); 15168597172@163.com (Z.J.); nianzh98@163.com (Z.N.); gyp@hdu.edu.cn (Y.G.)
[2] State Key Laboratory of Fluid Power and Mechatronic Systems, School of Mechanical Engineering, Zhejiang University, Hangzhou 310027, China
[3] Key Laboratory of 3D Printing Process and Equipment of Zhejiang Province, School of Mechanical Engineering, Zhejiang University, Hangzhou 310027, China
[4] Jiangsu Key Laboratory of 3D Printing Equipment and Manufacturing, Nanjing Normal University, Nanjing 210000, China
* Correspondence: shaohf@zju.edu.cn
† These authors contributed equally to this work.

Abstract: Intramedullary nails (INs) have significant advantages in rigid fracture fixation. Due to the stress shielding effect and lack of biological activity, traditional metal INs often lead to delay union or nonunion fracture healing. Undegradable metals also need to be removed by a second surgery, which will impose a potential risk to the patient. Current degradable biomaterials with low strength cannot be used in INs. Manufacturing high-strength biodegradable INs (BINs) is still a challenge. Here, we reported a novel high strength bioactive magnesium-containing silicate (CSi-Mg) BIN. This BIN is manufactured by using casting, freeze drying, and sintering techniques and has extremely high bending strength and stable internal and external structures. The manufacturing parameters were systematically studied, such as the paste component, freeze-drying process, and sintering process. This manufacturing method can be applied to various sizes of BINs. The CSi-Mg BIN also has good bioactivity and biodegradation properties. This novel bioactive BIN is expected to replace the traditional metal INs and become a more effective way of treating fractures.

Keywords: bioceramic; intramedullary nails; high strength; magnesium-containing silicate; fracture

check for updates

Citation: Ye, Y.; Shao, H.; Jing, Z.; Nian, Z.; Gong, Y. Magnesium-Containing Silicate Bioceramic Degradable Intramedullary Nail for Bone Fractures. *Crystals* **2022**, *12*, 974. https://doi.org/10.3390/cryst12070974

Academic Editor: Michele Iafisco

Received: 24 June 2022
Accepted: 9 July 2022
Published: 12 July 2022

Publisher's Note: MDPI stays neutral with regard to jurisdictional claims in published maps and institutional affiliations.

Copyright: © 2022 by the authors. Licensee MDPI, Basel, Switzerland. This article is an open access article distributed under the terms and conditions of the Creative Commons Attribution (CC BY) license (https://creativecommons.org/licenses/by/4.0/).

1. Introduction

About 10 million fractures occur worldwide every year, of which more than 60% are long bone fractures [1]. Intramedullary nails (INs) are widely used in the repair of long bone fractures due to their good mechanical structure and strength. They have gradually become the golden standards for the repair of long bone closure fractures due to the secondary healing outcomes and lower postoperative complications [2]. The most commonly used INs are made of stainless steel and titanium alloy [3]. The mechanical strength of these metal INs is generally higher than that of human bones, which can easily induce a stress shielding effect [4]. Chronic bone underloading can lead to adaptive responses and even bone resorption. This may be one of the main reasons for aseptic loosening of implants. In addition, the reduction in compressive load at the fracture site can inhibit the bone healing process [5]. Furthermore, metal INs lack the biological activity needed for bone tissue growth and have no excellent osteoinductive performance [6–8]. The biological activity refers to the characteristics of inducing special biological and chemical reactions on the interface between materials and biological tissues, which leads to the formation of chemical bonds between materials and biological tissues. Osteogenic properties are the properties of the surface or surrounding material that promote the formation of new bone. In addition,

they require a second operation to be removed because of their non-degradable properties in vivo, which not only increases the potential risk to the patient, but also causes additional costs and brings more pain to the patient [9]. Therefore, biodegradable implants represent attractive alternatives to conventional metal implants.

Driven by the demand for better healing of long bone fractures, ideal INs should have appropriate mechanical strength for initial stability, excellent biological activity and biodegradation properties for bone growth [10,11]. In the past few years, calcium silicate (CSi) ceramics have been extensively studied for use as implants in bone repair due to their excellent osteoconductivity and osteoinductivity [12,13]. However, the fast degradation rate, which cannot match the new bone formation speed [14] and is unfavorable for strength stability, and lower strength limit their further application in bone repair. Magnesium (Mg) is one of the essential elements in the human body and plays an important role in the bone marrow microenvironment. Recently, we have found that the calcium silicate ceramic doping with dilute magnesium (CSi-Mg) has improved mechanical strength and unexpected high fracture toughness [15]. The 3D-printed CSi-Mg scaffolds also have exhibited good elastic modulus and compressive strength which are similar to the mechanical properties of human bone [16]. The good mechanical properties can be obtained when 10% mol calcium (Ca) is substituted by magnesium in calcium silicate [17] and the CSi-Mg scaffold can promote the formation of new bone in the study of bone defects in the rabbit mandible and skull [18–20] due to the release of calcium, silicon, and magnesium ions during the degradation process [21], which is good for osteogenesis [22–24]. In addition, as the fourth trace element in the human body, Mg is critical for the IN-induced bone healing process [25,26]. Therefore, this new CSi-Mg ceramic has a broad application prospect in the fabrication of specific INs to enhance long bone regeneration and repair long bone fractures. However, the role of magnesium-containing calcium silicate ceramics in the repair of long bone fractures has not been systematically studied.

In order to solve the negative effects of conventional metal INs in long bone fracture repair, the researchers studied the variety of degradable biomaterials in recent years [27–29]. However, the demands for unique slender structure of the INs and extremely high mechanical strength are difficult to meet [30–32]. Furthermore, the manufacturing technique of biodegradable IN still needs to be improved, and a good universal manufacturing technique for fabricating high-strength biodegradable IN is needed as well.

Herein, a new fabrication method for high-strength and biodegradable magnesium-containing wollastonite IN is developed in this paper. Our objective is to investigate the effect of different manufacturing parameters such as paste component, freeze-drying process, and sintering process on the mechanical strength of INs. In addition, the possibility of high-strength degradable CSi-Mg INs for clinical application is also discussed. Through this method, biodegradable intramedullary nails can effectively solve the defects of metal intramedullary nails such as stress shielding failure.

2. Materials and Methods

2.1. Synthesis of CSi-Mg Powders

The CSi-Mg powders were synthesized using a conventional chemical co-precipitation method [15]. First, 10% mol Ca was substituted by Mg in wollastonite. Briefly, $Ca(NO_3)_2{\cdot}4H_2O$ and $Na_2SiO_3{\cdot}9H_2O$ were separately dissolved in deionized water in the concentration of 0.6 mol/L with a 10% mol proportion of $Ca(NO_3)_2$ replaced by $Mg(NO_3)_2$. Then, the Na_2SiO_3 solution was dropped into the $Ca(NO_3)_2/Mg(NO_3)_2$ solution mixture under continuous stirring and the pH value was maintained at 10.0–10.5. The powder precipitate was filtered, washed three times with deionized water, and finally washed using ethanol. The powder was dried at 70 °C, and then calcined at 920 °C for 180 min. All the chemical materials were purchased from Sinopharm Chemical Reagent Co., Ltd. The as-calcined CSi-Mg powders were ground in a planetary ball miller (MP-2L; Chishun Sci&Tech Co., Nanjing, China) using 3.5 mm diameter zirconia ball media in ethanol for 6 h and the average particle size of the resulting powders was below 5 μm.

2.2. Preparation of BINs

The BIN was fabricated using casting, freeze drying, and sintering techniques. Firstly, the paste was prepared by mixing CSi-Mg powders with polyvinyl alcohol (PVA, Sigma-Aldrich, Shanghai, China) solution (6% *w/v* or 15% *w*/*v*), and then was injected into the hollow glass tube mold, which was designed and fabricated in advance according to the size of BIN. Secondly, the molds filled with paste were pre-treated using the freeze-drying process at a low temperature for several hours, and then lyophilized overnight. Two main freeze-drying processes were conducted: slow freeze and quick freeze (half an hour or 3 h). Slow freeze was performed by controlling the temperature drop from room temperature to −80 °C in the vacuum freeze dryer (Lijahm Co., Shanghai, China) while quick freeze was carried out by keeping the temperature at −80 °C. Thirdly, the mold was removed, and the BIN samples were sintered in a micro-controller controlled-temperature furnace (Hefei Kejing Co., Hefei, China). Two main sintering routes were conducted including one-step sintering (OSS) and two-step sintering (TSS) methods. OSS was performed by sintering at a target temperature of T (1150, 1200, or 1225 °C) with a heating rate of 3 °C/min in air atmosphere using similar heating schemes, and held at the target temperature for 3 h, followed by cooling to 400 °C at a rate of 5 °C/min and finally cooled to room temperature naturally. TSS was carried out in three heating regimes. Samples were fired up to the higher target temperature (T_1 = 1200 or 1225 °C), with heating rate of 3 °C/min in air atmosphere, and held at T_1 for three time lengths (t = 15, 45, or 60 min), then rapidly cooled down to the lower temperature (T_2 = 1110 or 1150 °C) within 10 min and finally held at T_2 for 3 h. The BINs of 2.3, 7.5, and 12.8 mm in diameter were fabricated.

2.3. Physicochemical Characterization of the Bioceramic Powders and BIN

The phase composition of the CSi-Mg powders was verified by X-ray diffractometer (XRD; Rigaku Co., Tokyo, Japan) at 40 kV/40 mA. Data were collected between 5° and 80° with a step of 0.02°/2θ and a dwell time of 1.5 s to identify any crystalline phase of the powders. The inorganic ion content in CSi-Mg powder was measured by inductively coupled plasma-optical emission spectrometry (ICP-OES; Thermo Icap 6000 series, Waltham, MA, USA). The powders were observed by using the scanning electron microscopy (SEM, S-4800; Tokyo, Japan) at 10 kV. The particle size distribution was analyzed by dynamic light scattering (DLS, Malven Instrument 2000, Shanghai, China) in purified water medium. The shrinkage was determined by measuring the size of BINs before the freeze-drying process and after sintering treatment using a sliding caliper (inner diameter of the mold and diameter of the BIN). Six BIN samples were used for replicates of this test.

2.4. Mechanical Test of BIN

All the BIN samples (diameter of 2.3 mm and length of 40 mm) were subjected to a three-point bending test. A universal testing machine (Instron 5566, Shanghai, China) was used to test the bending strength of the BIN samples. The constant crosshead speed was 0.5 mm/min and the supporting span was 20 mm. Six BIN samples were used for replicates of this test.

2.5. Biodegradation Testing In Vitro

The BIN samples were soaked in Tris buffer with an initial pH of 7.4 in a shaking water-bath at 37 °C according to a surface area/volume ratio of 0.1 cm^{-1} in tubes. The samples (n = 6) were retrieved to measure the weight loss, bending strength, and the remaining soaking solutions were used for examination of the calcium, silicon, and magnesium concentrations and the pH values at 0, 1, 2, 3, 4, 5, and 6 weeks. To measure the dry weight, all the samples were dried at 80 °C for 24 h. The percentage weight loss was calculated as follows: weight loss (%) = $(w_0 - w_t)/w_0 \times 100\%$, where w_0 denotes the dry weight of the initial specimen, and w_t denotes the dry weight of the specimen at day t. At each soaking period, the calcium, silicon, and magnesium concentrations and pH values of the solutions were examined using inductively coupled plasma-atomic emission spectrometry (ICP-ACE,

Optima 2100, PerkinElmer, Waltham, MA, USA) and an electrolyte-type pH meter (FE20K, Mettler Toledo, Zurich, Switzerland).

2.6. Cell Viability In Vitro

Samples with a thickness of 1 mm and diameter of 10 mm were used in the cell culture. Bone marrow mesenchymal stem cells (BMSCs) were isolated and collected from Sprague-Dawley (SD) rats. Bone marrow was collected from the femurs and tibiae, and were then suspended in a growth medium containing α-modified Eagle's medium (α-MEM) (Gibco BRL, Bethesda, MD, USA) and 10% fetal bovine serum (FBS) (Gibco BRL, Bethesda, MD, USA), and cultured in a humidified atmosphere of 5% CO_2 at 37 °C. For the subculture, the cells were detached with 0.25% trypsin (Amresco, Solon, OH, USA) and 1 mM ethylene glycol bis (2-aminoethyl ether)-N,N,N′, N′-tetraacetic acid (EGTA) (Amresco, Solon, OH, USA) and were passaged when the cells grew to 70–80% confluence. All the experiments with the BMSCs were conducted with cultures at passage 3.

The BMSCs were seeded on the samples placed in the wells of 24-well plates at a density of 1×10^4 cells per well. After culturing for 1, 4, and 7 days, the Cell Counting Kit-8 (CCK-8, Dojindo, Kumamoto, Japan) assay was used to count the cells and analyze cell viability. A volume of 0.5 mL of α-MEM containing 10% CCK-8 was added into each well. After 2 h, 100 mL of the above-mentioned solution was transferred to a 96-well plate. A microplate reader (Infinite F50, TECAN, Hombrechtikon, Switzerland) was used to measure the absorbance at 450 nm. The absorbance value of a mixture of 90 mL of α-MEM and 10 mL of CCK-8 was subtracted as the background absorbance.

2.7. Statistical Analysis

All the data above were expressed as the mean value ± standard deviation (SD) and analyzed with the one-way analysis of variance (ANOVA). In all cases, the results were considered statistically significant at a p-value < 0.05.

3. Results and Discussion

3.1. Primary Characterization of the Bioceramic Powders and BINs

The BINs were fabricated as shown in the schematic diagram in Figure 1. We proposed for the first time to manufacture ceramic BIN with high strength by casting, freeze-drying process, and sintering process. It is a universal manufacturing method and can be widely used in the fabrication of other inorganic ceramic INs.

Figure 2A shows the SEM observation results. It can be seen that the particle sizes of CSi-Mg powders after calcination are all less than 5 μm. Evaluation of the particle size distribution conducted using DLS revealed a narrow size distribution in the range of 900–1700 nm for CSi-Mg (Figure 2B). These measurements are consistent with the SEM observation. Additionally, it is worth noting that the measured Mg content in CSi-Mg powder was 2.09 wt%, which was close to the theoretical data (2.12 wt%) calculated using the 10% Ca substitution by Mg in the stoichiometric wollastonite.

Figure 3 shows the XRD patterns of the CSi-Mg samples after different sintering temperatures. The spectral data confirmed that the CSi-Mg sample (1150 °C) has high crystallinity, which coincides with the wollastonite-2M (β-CSi; PDF# 27-0088), indicating pure wollastonite nature (Figure 3A). Moreover, the XRD pattern of the CSi-Mg sample sintered at 1225 °C was identical to that sintered at 1150 °C (Figure 3B), which is consistent with our previous result [15].

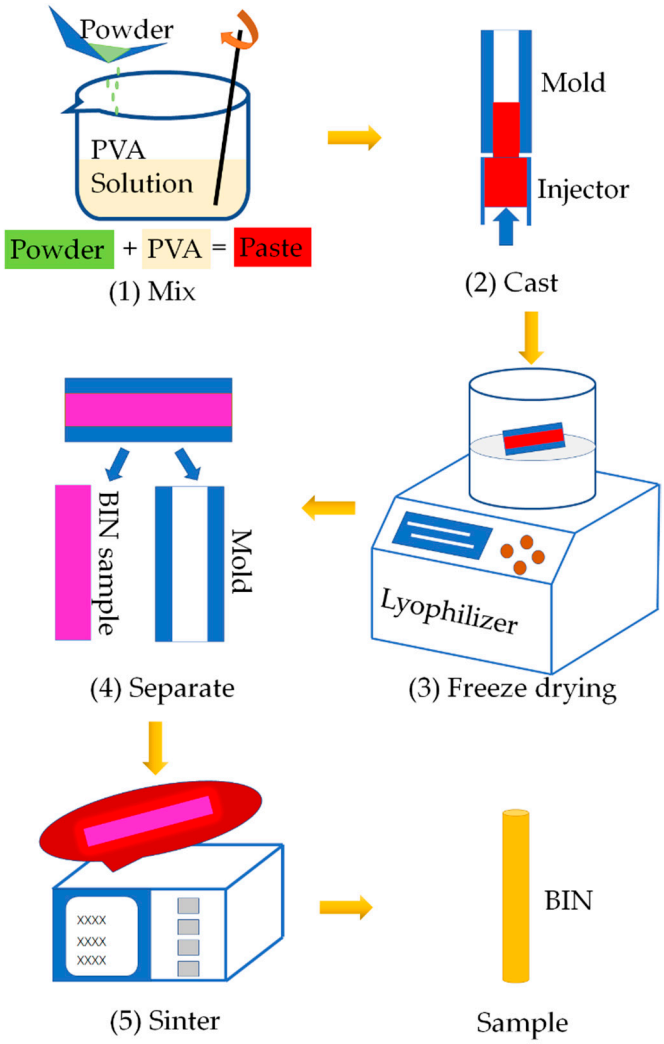


Figure 1. Schematic illustration of the manufacturing process of BINs. (1) Mixing CSi-Mg powders with PVA solution. (2) Pouring the paste into the hollow glass tube mold. (3) Freeze drying. (4) Demolding. (5) Sintering.

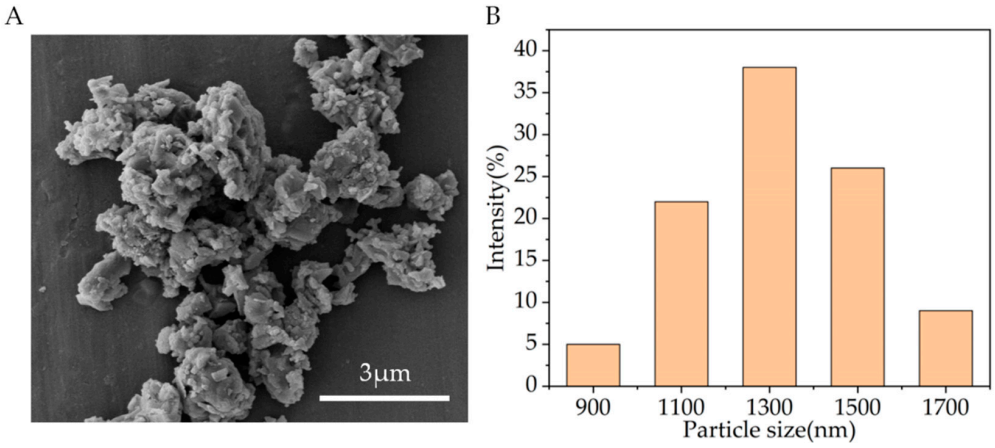


Figure 2. Characterization of the CSi-Mg powders. (**A**) SEM image of the CSi-Mg powders. (**B**) Particle size distribution of the powders.

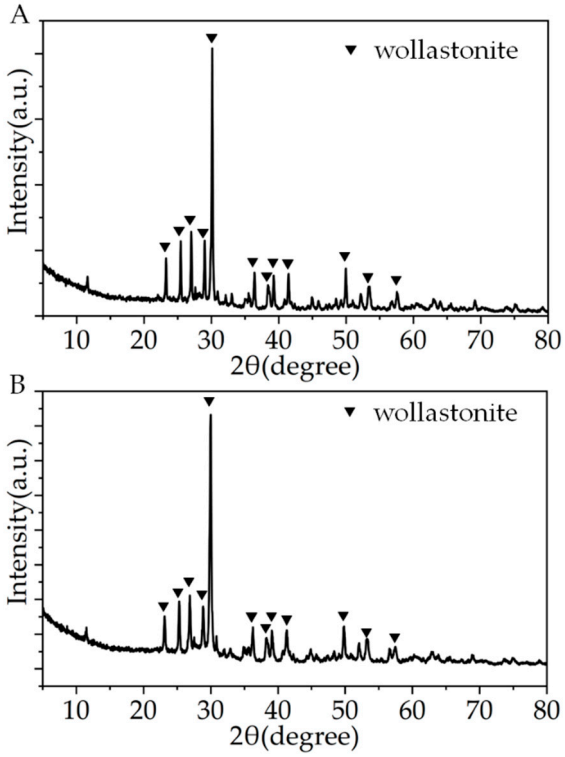


Figure 3. XRD patterns of the CSi-Mg samples sintered at 1150 °C (**A**) and 1225 °C (**B**).

Due to the special structure of IN, such as slender shape, it is difficult to manufacture IN with good straightness and uniformity. We have tried a lot of different manufacturing methods to fabricate INs. For example, we once used a casting and sintering process to manufacture IN. The paste was also injected into a hollow tube mold. However, the mold was used as the sacrifice material. The molds filled with paste were sintered together and the molds disappeared during the sintering process. However, it is difficult to obtain a slender shape of IN, most of which break down into several parts in the middle. Some other manufacturing methods can fabricate IN with complete structure, but there were some problems, such as the shape of IN is not straight, or the cross section of the IN is not uniform. The freeze-drying process can make the sample easier to demold and the composition of the sample is uniform due to the rapid freezing caused by low temperature. The manufacturing method in this paper overcomes the above problems and can fabricate the IN with good straightness and uniformity.

In the implementation of casting, freeze drying, and sintering processes, the process parameters, such as the paste composition, the time of freeze drying, freeze-drying processing procedures, and sintering temperature, have a great influence on the performance of the final BIN sample, especially on sample shrinkage, straightness, and mechanical strength. Therefore, the effects of these process parameters on the performance of the BIN samples were gradually investigated. For example, we studied the cooling process of the sintering process. The images of BINs with different cooling processes are shown in Figure 4. In the conventional sintering process, the sample is cooled to room temperature naturally while in our sintering process, the sample is cooled to 400 °C at a rate of 5 °C/min and then cooled to room temperature naturally. Figure 4A shows the BINs fabricated using the conventional sintering process. It can be seen that the shapes of the BINs are all curved. It is caused by the fast and nonuniform cooling rate in the conventional sintering process, especially for the slender sample. Additionally, with our gradual cooling method, the BINs have good straightness (Figure 4B). However, as shown in Figure 4B, the cross section of the BIN is not uniform, and the BIN is still defective. By optimizing the freeze-drying process, the BIN with good uniformity and straightness can be fabricated as shown in Figure 4C.

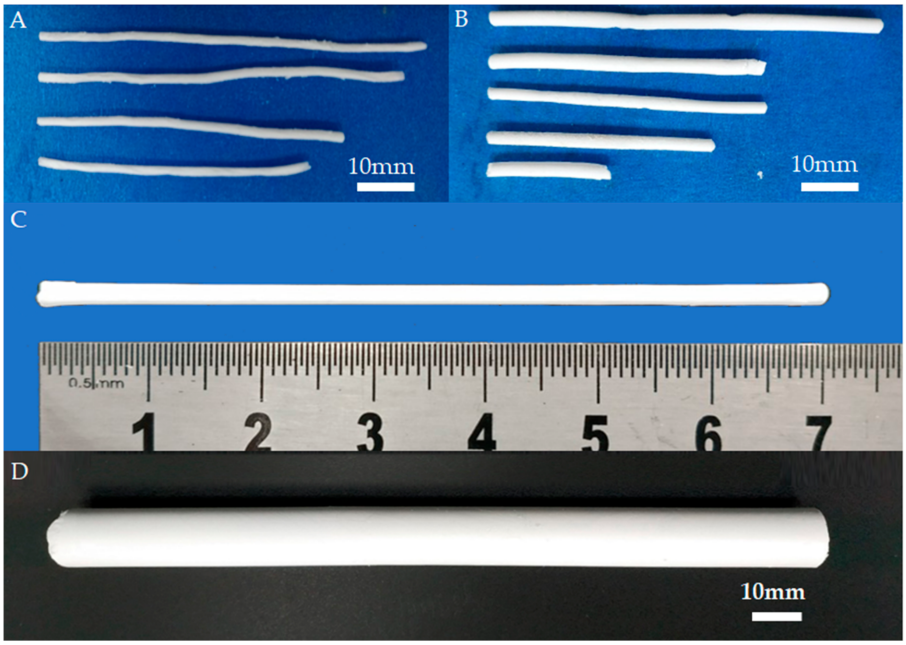


Figure 4. BIN image without (**A**) or with (**B**) cooling gradually in the sintering process. (**C**) Outward appearance of the as-sintered BIN after the optimized freeze-drying process. (**D**) The image of BIN with a diameter of ~12.8 mm and length of ~154 mm.

As we know, fractures can occur in different parts of the body and in different age groups, and the size requirement for BINs is different in each case. We also fabricated BIN with a larger size, as shown in Figure 4D. The diameter of BIN is 12.8 mm and the length of BIN is about 154 mm. This size is close to that of a clinical metal IN. The BIN with a larger size also has good straightness and uniformity. The BINs of large size are expected to be used in the clinic. During the fabrication process, the BIN sample will undergo two significant contractions. The first contraction occurs during the freeze-drying process and the second contraction occurs during the sintering process. Shrinkage is divided into diameter shrinkage and length shrinkage. The shrinkage in diameter is determined by measuring the diameter of BIN before the freeze-drying process and after sintering treatment using a sliding caliper. Additionally, the diameter of BIN before the freeze-drying process is the inner diameter of the mold. The shrinkage in length is also determined by measuring the length of the BIN before the freeze-drying process and after sintering treatment. According to the final size of BIN and shrinkage, we can customize the mold of the corresponding size. Therefore, we can fabricate BINs with different sizes (diameter and length) by applying molds of different sizes. This result indicated that BINs of any size can be fabricated using our fabrication method. Additionally, by changing the powder material, we can also fabricate INs of other materials such as hydroxyapatite and tricalcium phosphate.

3.2. Effect of Freeze-Drying Process on the Mechanical Property

The bending strength of the BINs (diameter of 2.3 mm) with 15% PVA solution, sintering schedule (OSS2), and different freeze-drying process (quick freeze for half an hour, quick freeze for 3 h, and slow freeze) is shown in Figure 5. The BINs made by slow freezing technique had an appreciable strength (~3.6 MPa) while the BINs made by quick freezing technique had higher bending strength. The bending strength of the BINs made by quick freezing technique increased with the increase in freezing time. When quick frozen for 3 h, the BINs showed higher bending strength (~8.5 MPa) than those slow frozen or quick frozen for half an hour. This value is 1.37 times higher than the strength of the BINs made by quick freezing technique for half an hour. The BINs made by slow freezing technique have lower bending strength caused by the nonuniformity within the BINs during the slow

freezing process (from room temperature to −80 °C). When quick frozen at −80 °C, the material is distributed evenly throughout the BINs.

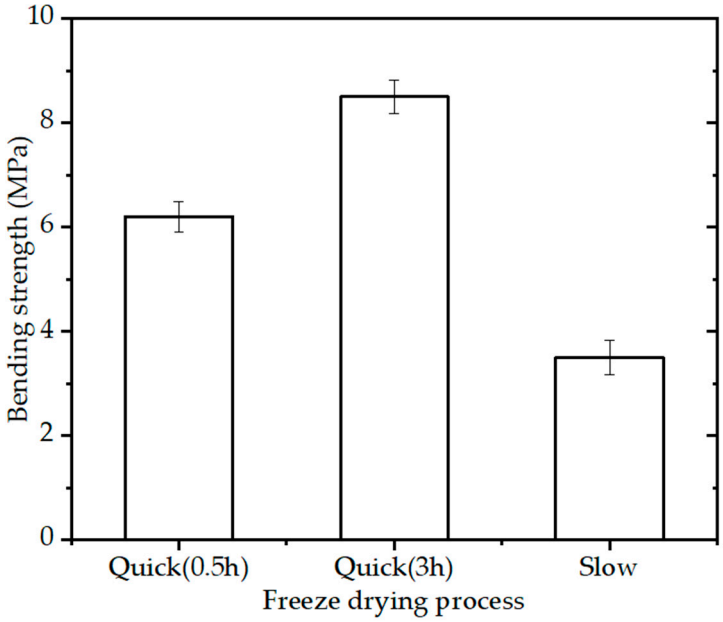


Figure 5. Bending strength of the BINs with different freeze-drying processes after one-step sintering at 1200 °C for 3 h ($p < 0.05$).

3.3. Effect of Paste Component on the Mechanical Property

The paste is composed of CSi-Mg powders and PVA solution and the composition of paste has an important effect on the final mechanical properties of BINs. For the same viscosity, the paste with lower mass fraction of PVA solution had higher content of CSi-Mg powders. A further evaluation involving the paste component on the mechanical strength needs to be investigated. The representative paste formulations are provided in Table 1.

Table 1. Chemical composition of the paste.

Samples	CSi-Mg (g)	PVA Solution (15%; g)	PVA Solution (6%; g)
15% PVA	4.0	4.0	-
6% PVA	5.0	-	4.0

Figure 6 shows the bending strength of the BINs (diameter of 2.3 mm) with different paste components, sintering schedule (OSS2), and quick freeze for 3 h. It can be seen that the BINs with 15% PVA solution have high bending strength (~8.5 MPa). As for the BINs with 6% PVA solution, Figure 6 shows that the bending strength of the BINs is ~41.7 MPa, which is 4.91 times higher than the bending strength of the BINs with 15% PVA solution. This may be caused by the content of CSi-Mg powders in paste. The content of CSi-Mg powders in the paste with 6% PVA solution was higher than that in the paste with 15% PVA solution. The result suggests that the paste component of the BINs is another important factor in influencing its mechanical properties.

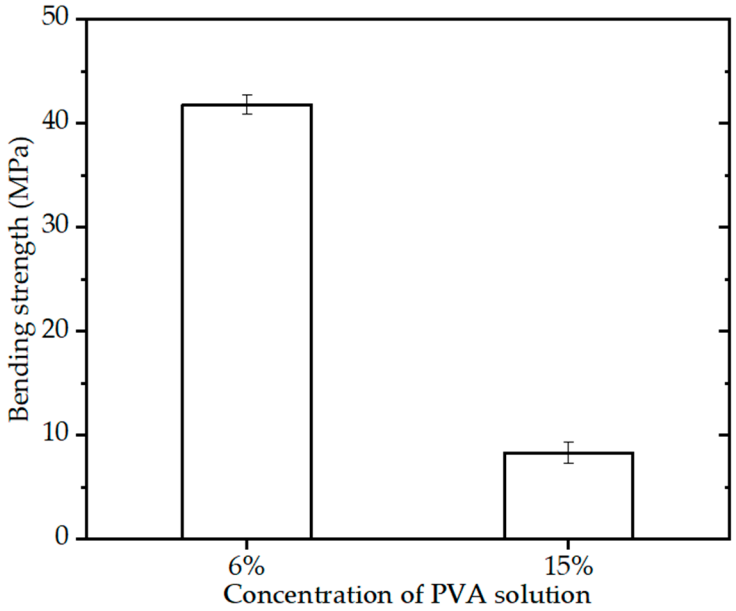


Figure 6. Bending strength of the BINs with different paste component after one-step sintering at 1200 °C for 3 h ($p < 0.05$).

3.4. Effect of Sintering Process on the Mechanical Property

The final mechanical properties of BINs are directly affected by the sintering process. Different sintering temperature and heating schedule will lead to different adhesion between the powders inside the BIN and different density of the BIN. Sintering, as an important treatment stage in ceramic processing, has undergone significant modifications and some novel sintering technologies and routes have been widely introduced. For example, pressure sintering, such as hot pressure and spark plasma sintering, is used to control the growth of Ca-silicate grain during extremely high rates of heating process [33–35]. However, it would need special equipment. It has been widely found that the TSS method can control the grain growth of ceramics during the final-stage sintering process [36]. The sintering under different TSS regimes can also be used to investigate the effect of sintering parameters on the densification behavior and grain growth suppression, which eventually contributes to the enhancement of mechanical strength [37,38]. In this study, we used one-step sintering and two-step sintering as two different heating schedules to investigate the effect on the mechanical strength of the BINs (diameter in 2.3 mm, 6% PVA solution, and quick freeze for 3 h). The sintering parameters and bending strength are shown in Table 2.

Table 2. List of sintering parameters and bending strength for OSS and TSS regimes.

Heat Regime	T1 (°C)	t1 (min)	T2 (°C)	t2 (h)	Bending Strength (MPa)
OSS1	1150	180	0	0	25.2 ± 0.9
OSS2	1200	180	0	0	41.7 ± 1.8
OSS3	1225	180	0	0	37.5 ± 1.1
TSS1	1200	45	1110	3	32.8 ± 1.3
TSS2	1200	45	1150	3	39.7 ± 1.6
TSS3	1225	45	1150	3	42.1 ± 2.1
TSS3	1225	60	1150	3	41.1 ± 1.9
TSS3	1225	15	1150	3	32.8 ± 1.1

The bending strength of the BINs sintered at 1150 °C is low (~25.2 MPa). Upon increasing the sintering temperature to 1200 °C, the BINs showed a significant high bending strength (~41.7 MPa), which was approximately 1.65 times higher than those for the BINs

sintered at lower temperature. When the sintering temperature was increased up to 1225 °C, the bending strength of the BINs decreased, but they still had a high value (~37.5 MPa). This result may be related to the grain size inside the BINs [14,20]. The bending strength of the BINs decreased with the increase in grain size sintered at 1225 °C. Furthermore, the BINs sintered at different temperatures showed similar shrinkage (~76.7%), and there was no significant difference. As follows from the above data, the BINs had high bending strength sintered at 1200 °C.

Data from the bending test of the BINs after undergoing different sintering conditions revealed that, after being held at 1200 °C for 45 min and then kept at 1150 °C for 3 h, the BINs had high bending strength (~39.7 MPa), which was 1.21 times higher than the BINs held at 1200 °C for 45 min and then kept at 1110 °C for 3 h, probably due to the low degree of densification of the latter. Additionally, if the first holding temperature was increased to 1225 °C, the BINs had a higher bending strength (~42.1 MPa), probably due to the better sintering properties and densification [39].

The BINs had a bending strength (~32.8 MPa) after being held at 1225 °C for 15 min and then kept at 1150 °C for 3 h. If the first holding time was prolonged to 45 min, the BINs displayed a significant enhancement in bending strength (~42.1 MPa). Additionally, if the first holding time was prolonged to 60 min, the bending strength of BINs decreased to ~41.1 MPa, which was still 1.25 times higher than the strength held at 1225 °C for 15 min. This result may be due to the fact that when the holding time was 15 min, the BINs were undersintering, but when the holding time was prolonged to 60 min, the bioceramic grain grew up and the BINs were oversintering. These data suggest that TSS is beneficial for the improvement of the mechanical strength of the BINs. However, there is no significant difference between the OSS and TSS methods.

3.5. Biodegradation Testing In Vitro

Figure 7A shows the biodegradation testing in vitro. Figure 7B–D show the pH, weight loss, inorganic ion-release concentrations, and bending strength in 6 weeks. During the degradation period, the Ca, Si, and Mg ions were gradually released as the materials degraded. At the same time, the weight loss gradually increased to 8.2%, the pH value gradually increased from about 7.4 to about 7.8, and the bending strength reduced from 41.7 to 18.7 MPa. At the end of the period, the release of Ca was the largest, reaching 243.32 ± 10.19 ppm, while Si was 83.16 ± 5.12 ppm and Mg was 22.06 ± 3.17 ppm. The BIN could stably release calcium, silicon, and magnesium ions, which are beneficial to osteogenesis.

The change in weight as a function of immersion time is shown in Figure 7B. The BINs have a high rate of weight loss within 4 weeks. The weight of all BINs reduced to 94.7–95.1% within the initial 2 weeks and reduced to 91.7–92.5% within 4 weeks. After 4 weeks, the rate of weight loss slowed. The weight of all BINs reduced to 91.4–92.2% after 6 weeks.

The pH value of the degradation solution changed from 7.4 to 7.8, with a very slight change of 0.4. The pH of the solution changed slightly to alkaline. We speculated that this change may be due to the chelation of SiO_4^{4-} released by BIN with the H^+ in the solution. Studies have shown that slightly alkaline micro-environments can increase osteoblast activity and proliferation [21]. However, when inorganic ions released by bioactive glass make the pH value of the cell growth fluid too high, the cells will undergo apoptosis [21]. Therefore, a limited increase in pH is beneficial for the growth of osteoblasts.

As for the strength decay during this process, the bending strength of BIN scaffolds decreased by half within 4 weeks, from ~41.7 MPa to ~19.8 MPa, and then maintained a very slow reduction. The BINs still have an appreciable bending strength (~18.7 MPa) after the whole immersion stage of 6 weeks. Therefore, the BINs show good mechanical stability.

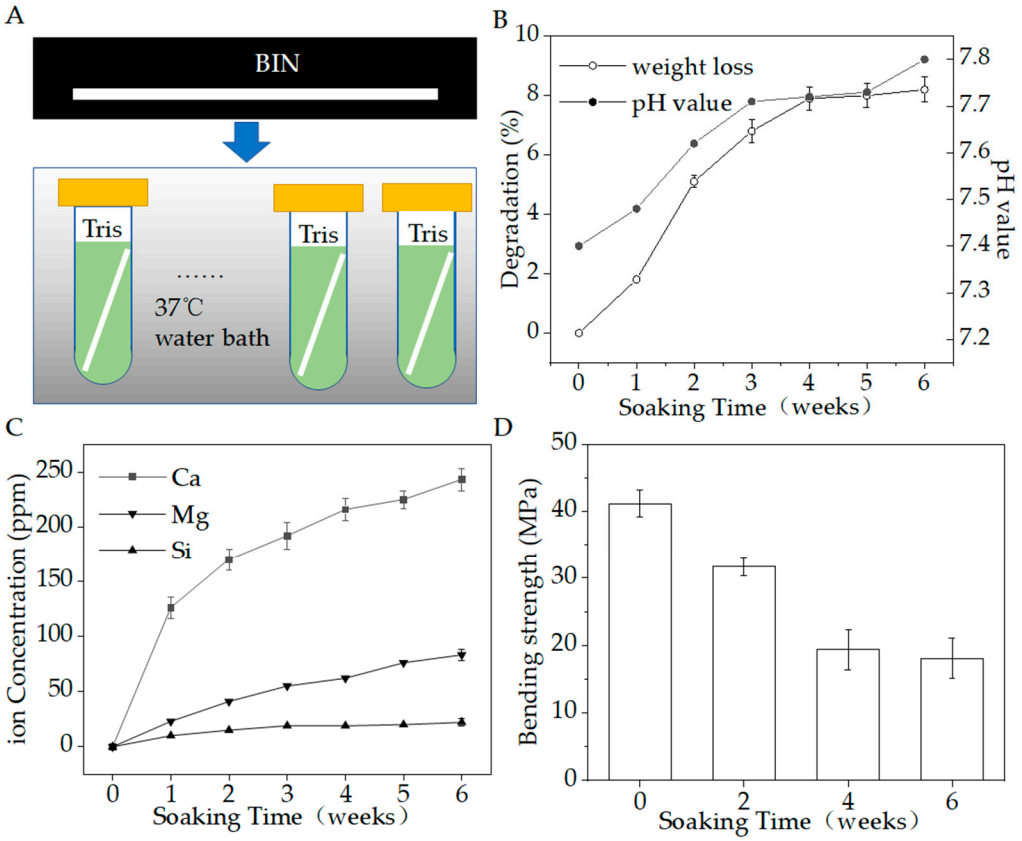


Figure 7. (**A**) Degradation in vitro. (**B**) Weight loss (%) and pH value during the degradation period. (**C**) Ions release during the degradation period. (**D**) Bending strength during the degradation period ($p < 0.05$).

3.6. Cell Viability In Vitro

Figure 8 shows cell viability in vitro. The Cell Counting Kit-8 (CCK8) was used to determine the Bone Marrow Mesenchymal Stem cells (BMSCs) viability on the samples after incubation for 1, 4, and 7 days. The group with the cells on the BIN showed a significantly higher viability than the control group at 7 days ($p < 0.05$). There was no significant difference among the groups at 1 and 4 days. This result showed that the CSi-Mg ceramic group could promote the cell viability of BMSCs.

The application of INs in fractured areas requires high bending strength. The current degradable materials have low mechanical strength, which limited their application in the clinic [40]. The CSi-Mg ceramics have excellent mechanical properties. According to our fabrication method with optimized process parameters, we can fabricate high bending strength BINs using CSi-Mg ceramic with OSS or TSS sintering method. Additionally, in the study on bone defects in rabbit mandible and skull [18–22], we found that the CSi-Mg ceramic can promote the formation of new bone and facilitate osteogenesis due to the release of calcium, silicon, and magnesium ions during the degradation process. They also have controlled biodegradation properties and good mechanical properties in vivo. Furthermore, we can also fabricate BINs of various sizes, which is suitable for clinical application. These results indicate that the novel biodegradable CSi-Mg INs have a good application prospect in future fracture repair.

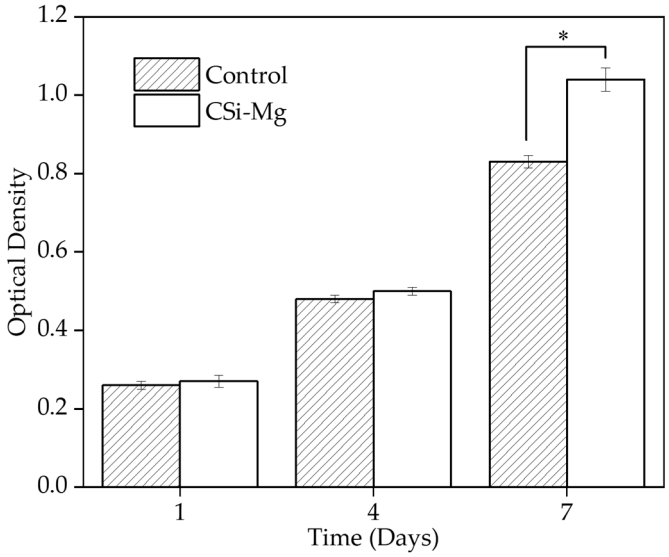


Figure 8. Cell viability at 1, 4, and 7 days (* $p < 0.05$).

4. Conclusions

In summary, a casting, freeze drying, and sintering processing strategy for fabricating a new biodegradable ceramic IN was developed in this study. The BINs had good straightness and uniformity. BINs with different sizes (diameter and length) can be fabricated using our fabrication method. The BIN had a high bending strength (>42 MPa) after optimizing the paste component, freeze-drying process, and sintering process. The biodegradation test and cell culture test also show that the BIN has good biodegradation properties and bioactivity. This finding suggests that our CSi-Mg BIN is promising for fracture repair. In addition to fabricating CSi-Mg BINs, our approach is ideally suited for fabricating a wide range of inorganic ceramic structures with controlled size and mechanical properties, which is needed for patients with different bone areas.

Author Contributions: Conceptualization, H.S.; methodology, Y.Y.; validation, H.S.; formal analysis, Z.J. and Z.N.; investigation, H.S. and Y.Y.; data curation, Z.J.; writing—original draft preparation, Y.Y. and Z.J.; writing—review and editing, Y.Y., Z.J. and H.S.; supervision, H.S.; project administration, Y.G.; funding acquisition, H.S. All authors have read and agreed to the published version of the manuscript.

Funding: This work was supported by the National Natural Science Foundation of China (grant number 51805475), Zhejiang Provincial Natural Science Foundation of China (grant number LY22E050011), Open Foundation of the State Key Laboratory of Fluid Power and Mechatronic Systems (grant number GZKF-202102), Jiangsu Key Laboratory of 3D Printing Equipment and Manufacturing (grant number 3DL202105), Key R&D program of Shanxi Province (International Cooperation, grant number 201903D421019).

Institutional Review Board Statement: Not applicable.

Informed Consent Statement: Not applicable.

Data Availability Statement: Not applicable.

Conflicts of Interest: The authors declare no conflict of interest.

References

1. Popkov, A.V.; Popkov, D.A.; Kononovich, N.A.; Gorbach, E.N.; Tverdokhlebov, S.I.; Bolbasov, E.N.; Darvin, E.O. Biological activity of the implant for internal fixation. *J. Tissue Eng. Regen. Med.* **2018**, *12*, 2248–2255. [CrossRef] [PubMed]
2. Burkus, M.; Tömböl, F.; Wiegand, N.; Kretzer, A. Physeal-sparing unreamed locked intramedullary nailing for adolescent tibial fractures. *Injury* **2020**, *52*, S67–S73. [CrossRef] [PubMed]

3. Rahman, M.M.; Mani, R.; Haque, O.; Beg, M.O.; Hasan, H. Short Term Outcome of Closed Intramedullary Fixation with Titanium Elastic Nail in Displaced Femoral Shaft Fractures in Skeletally Immature Children. *EAS J. Orthop. Physiother.* **2021**, *3*, 6–11.
4. Wu, X.; Tian, W.; Wang, Z.; Li, H.; Wang, H. Biomechanical evaluation of osteoporotic fracture: Metal fixation versus absorbable fixation in Sawbones models. *Injury* **2019**, *50*, 1272–1276. [CrossRef] [PubMed]
5. Wang, C.; Li, X.; Chen, W.; Wang, C.; Guo, H. Three-dimensional finite element analysis of intramedullary nail with different materials in the treatment of intertrochanteric fractures. *Injury* **2020**, *52*, 705–712. [CrossRef]
6. Du, J.H.; Lin, S.X.; Wu, X.L.; Yang, S.M.; Jiang, X.Q. The Function of Wnt Ligands on Osteocyte and Bone Remodeling. *J. Dent. Res.* **2019**, *98*, 930–938. [CrossRef]
7. Maryam, T.; Ling, W.; Ziyu, L.; Chaozong, L. Osteochondral tissue repair in osteoarthritic joints: Clinical challenges and opportunities in tissue engineering. *Bio-Des. Manuf.* **2018**, *1*, 101–114.
8. Korhonen, L.; Perhomaa, M.; Kyro, A.; Pokka, T.; Serlo, W.; Merikanto, J.; Sinikumpu, J.J. Intramedullary nailing of forearm shaft fractures by biodegradable compared with titanium nails: Results of a prospective randomized trial in children with at least two years of follow-up. *Biomaterials* **2018**, *185*, 383–392. [CrossRef]
9. Vijayavenkataraman, S.; Gopinath, A.; Lu, W.F. A new design of 3D-printed orthopedic bone plates with auxetic structures to mitigate stress shielding and improve intra-operative bending. *Bio-Des. Manuf.* **2020**, *3*, 98–108. [CrossRef]
10. Kramer, M.; Schilling, M.; Eifler, R.; Hering, B.; Reifenrath, J.; Besdo, S.; Windhagen, H.; Willbold, E.; Weizbauer, A. Corrosion behavior, biocompatibility and biomechanical stability of a prototype magnesium-based biodegradable intramedullary nailing system. *Mater. Sci. Eng. C* **2016**, *59*, 129–135. [CrossRef]
11. Suda, A.J.; Brachtendorf, X.; Tinelli, M.; Wagokh, R.; Bischel, O.E. Low complication rate and better results for intramedullary nail-arthrodesis for infected knee joints compared to external fixator—A series of one hundred fifty two patients. *Int. Orthop.* **2021**, *45*, 1735–1744. [CrossRef]
12. Shao, H.; Yang, X.; He, Y.; Fu, J.; Liu, L.; Ma, L.; Zhang, L.; Yang, G.; Gao, C.; Gou, Z. Bioactive glass-reinforced bioceramic ink writing scaffolds: Sintering, microstructure and mechanical behavior. *Biofabrication* **2015**, *7*, 035010. [CrossRef]
13. Zhou, P.; Xia, D.; Ni, Z.; Ou, T.; Wang, Y.; Zhang, H.; Mao, L.; Lin, K.; Xu, S.; Liu, J. Calcium silicate bioactive ceramics induce osteogenesis through oncostatin M. *Bioact. Mater.* **2021**, *6*, 810–822. [CrossRef]
14. Wen, J.; Liao, J.; Ying, Q.; Li, H.; Zhu, Y.J. Improvement of in vitro degradation of magnesium oxychloride cement for bone repair by chitosan. *J. Mater. Sci.* **2021**, *56*, 706–717. [CrossRef]
15. Xie, J.; Yang, X.; Shao, H.; Ye, J.; He, Y.; Fu, J.; Gao, C.; Gou, Z. Simultaneous mechanical property and biodegradation improvement of wollastonite bioceramic through magnesium dilute doping. *J. Mech. Behav. Biomed. Mater.* **2016**, *54*, 60–71. [CrossRef]
16. Liu, A.; Sun, M.; Shao, H.; Yang, X. The outstanding mechanical response and bone regeneration capacity of robocast dilute magnesium-doped wollastonite scaffolds in critical size bone defects. *J. Mater. Chem. B* **2016**, *4*, 3945–3958. [CrossRef]
17. Xie, J.; Shao, H.; He, D.; Yang, X.; Yao, C.; Ye, J.; He, Y.; Fu, J.; Gou, Z. Ultrahigh strength of three-dimensional printed diluted magnesium doping wollastonite porous scaffolds. *MRS Commun.* **2015**, *5*, 631–639. [CrossRef]
18. Shao, H.; Sun, M.; Zhang, F.; Liu, A.; He, Y.; Fu, J.; Yang, X.; Wang, H.; Gou, Z. Custom Repair of Mandibular Bone Defects with 3D Printed Bioceramic Scaffolds. *J. Dent. Res.* **2018**, *97*, 68–76. [CrossRef]
19. Shao, H.; Ke, X.; Liu, A.; Sun, M.; He, Y.; Yang, X.; Fu, J.; Liu, Y.; Zhang, L.; Yang, G.; et al. Bone regeneration in 3D printing bioactive ceramic scaffolds with improved tissue/material interface pore architecture in thin-wall bone defect. *Biofabrication* **2017**, *9*, 025003. [CrossRef]
20. Shao, H.; Liu, A.; Ke, X.; Sun, M.; He, Y.; Yang, X.; Fu, J.; Zhang, L.; Yang, G.; Liu, Y.; et al. 3D robocasting magnesium-doped wollastonite/TCP bioceramic scaffolds with improved bone regeneration capacity in critical sized calvarial defects. *J. Mater. Chem. B* **2017**, *5*, 2941–2951. [CrossRef]
21. Shao, H.; He, Y.; Fu, J.; He, D.; Yang, X.; Xie, J.; Yao, C.; Ye, J.; Xu, S.; Gou, Z. 3D printing magnesium-doped wollastonite/β-TCP bioceramics scaffolds with high strength and adjustable degradation. *J. Eur. Ceram. Soc.* **2016**, *36*, 1495–1503. [CrossRef]
22. Sun, M.; Liu, A.; Shao, H.; Yang, X.; Ma, C.; Yan, S.; Liu, Y.; He, Y.; Gou, Z. Systematical evaluation of mechanically strong 3D printed diluted magnesium doping wollastonite scaffolds on osteogenic capacity in rabbit calvarial defects. *Sci. Rep.* **2016**, *6*, 34029. [CrossRef]
23. Tahmineh, A.; Ahmad, M.; Vajihsadat, M.; Mohammad, H.F. Fabrication and characterization of polycaprolactone fumarate/gelatin-based nanocomposite incorporated with silicon and magnesium co-doped fluorapatite nanoparticles using electrospinning method. *Mat. Sci. Eng. C-Mater.* **2020**, *106*, 110172.
24. Li, Z.; Zhang, X.; Ouyang, J.; Chu, D.; Han, F.; Shi, L.; Liu, R.; Guo, Z.; Gu, G.X.; Tao, W. Ca^{2+}-supplying black phosphorus-based scaffolds fabricated with microfluidic technology for osteogenesis. *Bioact. Mater.* **2021**, *6*, 4053–4064. [CrossRef]
25. Lin, S.; Yang, G.; Jiang, F.; Zhou, M.; Yin, S.; Tang, Y.; Tang, T.; Zhang, Z.; Zhang, W.; Jiang, X. A Magnesium-Enriched 3D Culture System that Mimics the Bone Development Microenvironment for Vascularized Bone Regeneration. *Adv. Sci.* **2019**, *6*, 1900209. [CrossRef]
26. Zhou, H.; Liang, B.; Jiang, H.; Deng, Z.; Yu, K. Magnesium-based biomaterials as emerging agents for bone repair and regeneration: From mechanism to application. *J. Magnes. Alloy.* **2021**, *9*, 779–804. [CrossRef]
27. Jahn, K.; Saito, H.; Taipaleenmaki, H.; Gasser, A.; Hort, N.; Feyerabend, F.; Schluter, H.; Rueger, J.M.; Lehmann, W.; Willumeit-Romer, R.; et al. Intramedullary Mg2Ag nails augment callus formation during fracture healing in mice. *Acta Biomater.* **2016**, *36*, 350–360. [CrossRef]

28. Wang, Z.; Wang, X.; Pei, J.; Tian, Y.; Zhang, J.; Jiang, C.; Huang, J.; Pang, Z.; Cao, Y.; Wang, X.; et al. Degradation and osteogenic induction of a SrHPO4-coated Mg-Nd-Zn-Zr alloy intramedullary nail in a rat femoral shaft fracture model. *Biomaterials* **2020**, *247*, 119962. [CrossRef]
29. Chaudhary, M.; Jain, T.; Jain, J.K. Advanced manufacturing techniques and advancements in biodegradable biomaterials. *Mater. Today Proc.* **2021**, *47*, 6686–6692. [CrossRef]
30. Ji, K.; Wang, Y.; Wei, Q.; Zhang, K.; Jiang, A.; Rao, Y.; Cai, X. Application of 3D printing technology in bone tissue engineering. *Bio-Des. Manuf.* **2018**, *1*, 203–210. [CrossRef]
31. Throop, A.D.W.; Clark, A.M.; Kuxhaus, L. An Adjustable-Length Intramedullary Nail: Development and Mechanical Evaluation in Cervine Tibiae. *J. Med. Devices* **2015**, *9*, 024503. [CrossRef]
32. Quinnan, S.; Seiter, M.; Al-Barghouthi, A.; Milne, E.; Travascio, F. Does coating an intramedullary nail with polymethylmethacrylate improve mechanical stability at the fracture site? *Clin. Biomech.* **2021**, *83*, 105293. [CrossRef] [PubMed]
33. Champion, E. Sintering of calcium phosphate bioceramics. *Acta Biomater.* **2013**, *9*, 5855–5875. [CrossRef] [PubMed]
34. Fu, L.; Engqvist, H.; Xia, W. Spark plasma sintering of biodegradable Si_3N_4 bioceramic with Sr, Mg and Si as sintering additives for spinal fusion. *J. Eur. Ceram. Soc.* **2017**, *38*, 2110–2119. [CrossRef]
35. Bazin, T.; Magnaudeix, A.; Mayet, R.; Carles, P.; Champion, E. Sintering and biocompatibility of copper-doped hydroxyapatite bioceramics. *Ceram. Int.* **2021**, *47*, 13644–13654. [CrossRef]
36. Silva, L.D.; Puosso, F.C.; Soares, V.O.; Filho, O.P.; Zanotto, E.D. Two-step sinter-crystallization of K_2O-CaO-P_2O_5-SiO_2 (45S5-K) bioactive glass. *Ceram. Int.* **2021**, *47*, 18720–18731. [CrossRef]
37. Nadernezhad, A.; Moztarzadeh, F.; Hafezi, M.; Barzegar-Bafrooei, H. Two step sintering of a novel calcium magnesium silicate bioceramic: Sintering parameters and mechanical characterization. *J. Eur. Ceram. Soc.* **2014**, *34*, 4001–4009. [CrossRef]
38. Lukić, M.; Stojanović, Z.; Škapin, S.D.; Maček-Kržmanc, M.; Mitrić, M.; Marković, S.; Uskoković, D. Dense fine-grained biphasic calcium phosphate (BCP) bioceramics designed by two-step sintering. *J. Eur. Ceram. Soc.* **2011**, *31*, 19–27. [CrossRef]
39. Hussain, A.M.; Haq, E.U.; Munawar, I.; Maqbool, A.; Saleem, M.; Rafiq, M.A.; Inam, A.; Hakeem, A.S. Influence of spark plasma sintering temperature and hydroxyapatite nanoparticles on properties of HA based functionally graded materials for bone prosthesis. *Ceram. Int.* **2022**, *48*, 14481–14490. [CrossRef]
40. Diba, M.; Goudouri, O.-M.; Tapia, F.; Boccaccini, A.R. Magnesium-containing bioactive polycrystalline silicate-based ceramics and glass-ceramics for biomedical applications. *Curr. Opin. Solid. State Mater. Sci.* **2014**, *18*, 147–167. [CrossRef]